

~10 km to the south from slope diffusion modeling (16). This age agrees within uncertainty with our age of 2.6 ka.

Our results indicate that most of the slip occurred at ~24 to 20 ka and 7 to 0 ka. These times of increased activity were separated by a period of relative seismic quiescence. A similar time interval separates the period of activity at 20 to 24 ka from the next older ³⁶Cl age of ~37 ka, suggesting that earthquake activity on the Hebgen Lake fault is periodic. This temporal clustering of paleo-earthquakes is similar to that described elsewhere for the Great Basin (17, 18) and suggested for other intraplate faults (19).

References and Notes

1. J. P. McCalpin, Ed., *Paleoseismology*, vol. 62 of *International Geophysics Series* (Academic Press, San Diego, CA, 1996).
2. J. S. Noller, J. M. Sowers, W. R. Lettis, Eds., *Quaternary Geochronology: Applications in Quaternary Geology and Paleoseismology* (American Geophysical Union, Washington, DC, in press).
3. W. B. Myers and W. Hamilton, *U.S. Geol. Surv. Prof. Pap.* 435, 58 (1964).
4. I. J. Witkind, *ibid.*, p. 37.
5. R. Davis Jr., and O. A. Schaeffer, *Ann. N.Y. Acad. Sci.* 62, 105 (1955).
6. F. M. Phillips, B. D. Leavy, N. O. Jannik, D. Elmore, P. W. Kubik, *Science* 231, 41 (1986).
7. M. G. Zreda et al., *Earth Planet. Sci. Lett.* 105, 94 (1991).
8. F. M. Phillips, M. G. Zreda, M. R. Flinsch, D. Elmore, P. Sharma, *Geophys. Res. Lett.* 23, 949 (1996).
9. B. Liu, F. M. Phillips, J. T. Fabryka-Martin, M. M. Fowler, R. S. Biddle, *Water Resour. Res.* 30, 3115 (1994).
10. J. O. H. Stone, J. M. Evans, L. K. Fifield, G. L. Allan, R. G. Cresswell, *Geochim. Cosmochim. Acta* 62, 433 (1998).
11. J. T. Fabryka-Martin, thesis, University of Arizona (1988).
12. R. G. Tysdal, *Geologic Map of the Sphinx Mountain Quadrangle and Adjacent Parts of the Cameron, Cliff Lake, and Hebgen Dam Quadrangles, Montana* (1-1815, U.S. Geological Survey, Washington, DC, 1990).
13. Rock samples were collected from top 2 to 5 cm of rock using hammer and chisel. The samples were cleaned of any organic material and encrustations, crushed and ground, and sieved to size fraction 0.25 to 1.00 mm. To remove any meteoric ³⁶Cl, they were leached first in 3% nitric acid for a few minutes and then in deionized water for 24 hours, dried in an oven overnight at 100°C, and placed in sterile plastic bags. Samples for ³⁶Cl were obtained by dissolution of 100 g of purified rocks in sufficient amount of 5% nitric acid mixed with 20 ml of 0.1 M AgNO₃. To prevent rapid sample dissolution and minimize possible loss of Cl with released CO₂, nitric acid was dispensed slowly (1 ml/min) using a pump. Chloride was precipitated as AgCl (12) [M. G. Zreda, F. M. Phillips, S. S. Smith, *Cosmogenic ³⁶Cl Dating of Geomorphic Surfaces (Hydrology Program Rep. 90-1, New Mexico Institute of Mining and Technology, 1990)*; M. G. Zreda, thesis, New Mexico Institute of Mining and Technology (1994)], which was rinsed in deionized water and purified of sulfur with barium nitrate. Chlorine-36 was measured by accelerator mass spectrometry [D. Elmore et al., *Nature* 277, 22 (1979)] at Purdue University. Major elements were determined by x-ray fluorescence or inductively coupled plasma-atomic emission spectrometry, and Cl by the ion-selective electrode method [P. J. Aruscavage and E. Y. Campbell, *Talanta* 30, 745 (1983)] modified for carbonate rocks.
14. Apparent cosmogenic ³⁶Cl surface exposure ages were calculated using CHLOE software [F. M. Phillips and M. A. Plummer, *Radiocarbon* 38, 98 (1996)], with spallation production rates of 73.3 ± 4.9 atoms ³⁶Cl

(g Ca)⁻¹ year⁻¹ and 154 ± 10 atoms ³⁶Cl (g K)⁻¹ year⁻¹ (8) and thermal neutron activation production rate calculated (9) from the fast neutron production rate of 586 ± 40 neutrons (g air)⁻¹ year⁻¹ (8). We used these production rates because they were determined from a large number of samples of different ages and from 15 separate locations; other production rate studies used single locations or small numbers of samples. These production rates are for sea level and high latitudes and were scaled [D. Lal, *Earth Planet. Sci. Lett.* 104, 424 (1991)] to the locations of sample sites. In addition, we accounted for muogenic production (10) below the surface and for topographic shielding by the scarp [M. G. Zreda and F. M. Phillips, in *Dating in Exposed and Surface Contexts*, C. Beck, Ed. (Univ. of New Mexico Press, Albuquerque, 1994), pp. 161-183]. We did not correct the production rates for temporal variability because doing so does not improve the uncertainty of the production rate estimates (8). Uncertainties of the ³⁶Cl ages are due to a combination of analytical errors and systematic errors associated with production rate calculations. These uncertainties are <15% for moraines

from which multiple rock samples per surface are analyzed [F. M. Phillips et al., *Geol. Soc. Am. Bull.* 109, 1453 (1997)]. Two additional sources of systematic error are related to production of ³⁶Cl below the surface and to topographic shielding by the scarp. The errors associated with these variables are not well known, but they are likely on the order of 10%.

15. See *Science Online* (www.sciencemag.org) for supplementary data on sample heights, ³⁶Cl production parameters, and cosmogenic ³⁶Cl ages for six different sections of the Hebgen fault scarp.
16. D. B. Nash, *Geol. Soc. Am. Bull.* 95, 1413 (1984).
17. R. E. Wallace, *J. Geophys. Res.* 89, 5763 (1984).
18. ———, *Seismol. Soc. Am. Bull.* 74, 301 (1987).
19. A. J. Crone and K. V. Luza, *Geol. Soc. Am. Bull.* 102, 1 (1990).
20. Supported by the Nuclear Regulatory Commission, the Packard Fellowship in Science and Engineering, and NSF. We thank W. Lettis for field assistance, R. Schapiro and D. Robinson for help in sample collection, and two anonymous reviewers for constructive comments.

2 July 1998; accepted 7 October 1998

Detection of Centimeter-Sized Meteoroid Impact Events in Saturn's F Ring

Mark R. Showalter

Voyager images reveal that three prominent clumps in Saturn's F ring were short-lived, appearing rapidly and then spreading and decaying in brightness over periods of ~2 weeks. These features arise from hypervelocity impacts by ~10-centimeter meteoroids into F ring bodies. Future ring observations of these impact events could constrain the centimeter-sized component of the meteoroid population, which is otherwise unmeasurable but plays an important role in the evolution of rings and surfaces in the outer solar system. The F ring's numerous other clumps are much longer lived and appear to be unrelated to impacts.

The faint and narrow F ring orbits 3000 km beyond the outer edge of Saturn's main ring system. It was discovered during the Pioneer 11 encounter in 1979 (1) but was imaged more clearly and extensively by Voyager's cameras in 1980 and 1981 (2, 3). The Voyager images revealed a variety of peculiar structures within the ring, variously described as strands, kinks, clumps, and "braids." Many of these structures are now believed to be related to gravitational perturbations by the nearby "shepherding" moons Prometheus and Pandora (4-6), but details of the interactions remain mysterious.

The F ring appears much brighter in forward-scattered than backscattered light, suggesting diffraction by a population of fine dust. Photometric models reveal the dust to be predominantly <1 μm in size (7). Such fine dust has a brief lifetime of 10³ to 10⁶

years against various drag forces and loss mechanisms (8), so it must be replenished by an unseen population of larger parent bodies.

After Voyager, the F ring was not seen again until 1995, during the crossings of Earth and sun through Saturn's ring plane. Observers reported a number of new moons near the F ring (9-11); however, with implied radii of ~10 km, these bodies were too large to have escaped detection by Voyager. They have integrated brightnesses comparable to that of the brightest clumps observed by Voyager (10), so clumps provide a much more plausible explanation for these "moons." The numbers and locations of the clumps changed between observations in May, August, and November of 1995 (9-11), suggesting that they are transient, with lifetimes <3 months.

The 1995 images provided a firmer constraint than the Voyager data set, which merely showed that no major clumps survived for the ~9 months between encounters (12). However, the Voyager data set is much more extensive than any obtainable from the ground, with reasonable resolution and nearly complete longitudinal coverage for periods of

Space, Telecommunications and Radioscience Laboratory, Stanford University, Stanford, CA 94305, USA. Mailing address: 245-3 NASA Ames Research Center, Moffett Field, CA 94035-1000, USA. E-mail: showalter@ringside.arc.nasa.gov

~50 days surrounding each encounter. Using analysis techniques introduced by Kolvoord *et al.* (6), I derived longitudinal profiles of the F ring's radially integrated intensity from each of 1500 images. By working in a frame rotating at the F ring's mean motion (13), features stay essentially fixed in location. Most images contain only a small segment of the ring, and signal-to-noise ratios are often very low, so profiles were grouped by time intervals and combined to improve longitudinal coverage and quality (14). The result is a sequence of profiles showing how individual clumps evolve during each encounter (15).

A pair of profiles from just before and just after Voyager 2's closest approach (Fig. 1) shows three major clumps labeled 2B, 2C,

and 2C' that were relatively stable for the intervening week, but a fourth, labeled 2A, appears to be new. A time series of profiles (Fig. 2A) shows that clump 2A appeared suddenly in ≤ 4 days and then spread longitudinally while decreasing in brightness over the next 5 days that it could be observed. Of 58 clumps, large and small, tracked in the ring profiles from both encounters, most show only very minor changes in shape and brightness over periods of 1 to 2 months (15). Only two other clumps, identified as 1C and 1J, show rapid changes like 2A (Fig. 2, B and C). The three clumps arise quickly (in periods of less than a few days), persist for ~15 days, and spread in full width by ~0.3° per day. When they first appear, they are among the

brightest ring features. I dub these "burst events." Given that events occurring within ~15 days of Voyager's closest approach are most likely to be observable, the frequency of burst events is estimated to be one every ~20 days.

The observed spreading rate of these features implies that the individual particles have random velocities of ~4 m/s. Assuming that the random velocities are distributed isotropically, the corresponding range of semi-major axes should be ~100 km. This value is several times the radial width of the brightest ring strand. Such an enhancement in radial width is in fact observed in clump 2A (Fig. 3, inset), the only one of these three events imaged at suitable resolution. The F ring's more common and stable clumps show no such enhancement in width.

The 4 m/s random velocity in these three events is typical of the ejecta from hypervelocity impacts (8). Such high random speeds cannot arise from mutual collisions between F ring bodies because the ring's core is only a few kilometers wide, so relative velocities are much lower. For comparison, the other more numerous clumps in the F ring (15) have longer lifetimes that are consistent with mutual collisions; these clumps most likely appear whenever two bodies collide and shed their loosely held coverings of dust (16, 17).

To release the high-speed ejecta observed in bursts, a source of impactors from outside

Fig. 1. Two complete longitudinal profiles of Saturn's F ring from the Voyager 2 encounter. Each panel shows the ring's radially integrated intensity or "equivalent width" as a function of longitude θ in a frame that corotates with the ring, with the mean motion derived by (13). The longitude reference is the ring plane's ascending node on Earth's equator of B1950; the time reference is Voyager's closest approach to the planet, 3:24:08 UT on 26 August 1981. Intensity I is specified by the dimensionless ratio I/F , where πF is the incident solar flux density. The top panel was derived from 28 images 4.8 days before the closest approach; the bottom panel is from eight images 3.0 to 4.5 days after the closest approach. The slight difference in overall amplitude of the profiles arises from the difference in phase angle. In general, most structures are unchanged between the two profiles, such as major clumps 2B, 2C, and 2C'. The one exception is an apparently new feature labeled 2A.

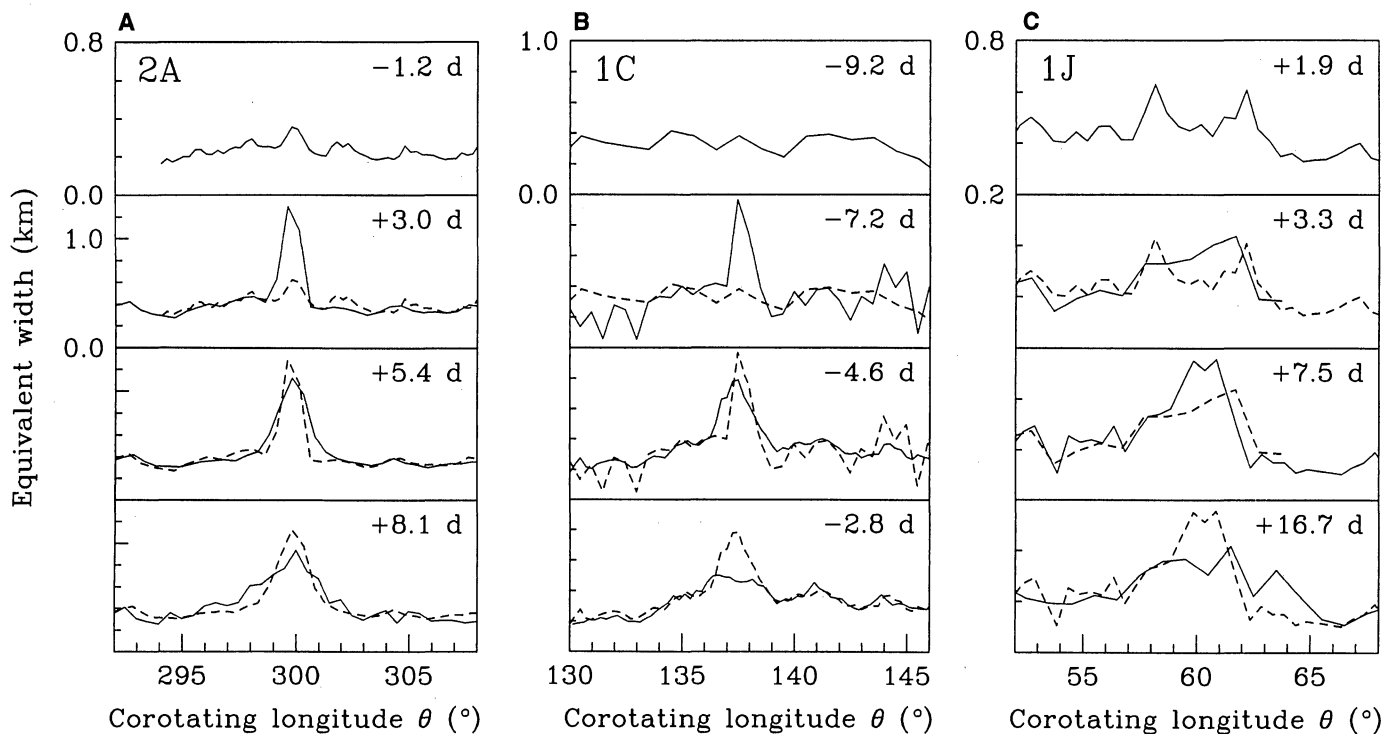
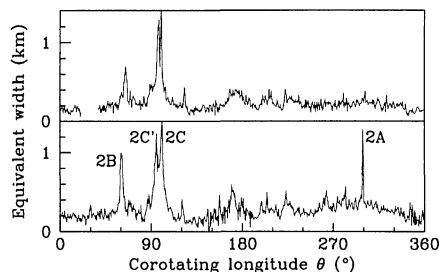


Fig. 2. A time series of profiles for three time-variable clumps, designated (A) 2A, (B) 1C, and (C) 1J. 2A is from the Voyager 2 encounter and 1C and 1J are from Voyager 1. Times relative to closest approach are given in units of days (d) at the top right corner of each panel. In each panel,

the curve from the panel above is repeated as a dashed line to facilitate comparisons. When the vertical scale of a panel is unlabeled, it is identical to that of the panel above; the scale changes between the first two time steps of clump 2A to compensate for a change in phase angle.

REPORTS

the F ring is required. The amount of dust released in a hypervelocity impact is related to the size of the impactor. Observations of 1C and 2A permit accurate photometry; both reflect light equivalent to that from a perfectly diffusing “Lambert” surface of area ~ 2 km². The phase angle is 14° for 1C and 95° for 2A. Converting this brightness to a volume of dust requires a model for the dust’s size distribution, shape, and composition, which are not well known. I modeled the differential size distribution $n(r)$ as a power law proportional to r^{-q} , for particle radii r between cutoffs of r_1 and r_2 (7). I considered $2.5 \leq q \leq 4.5$, $0.001 \mu\text{m} \leq r_1 \leq 1 \mu\text{m}$, and $1 \mu\text{m} \leq r_2 \leq 100 \mu\text{m}$ (18). Shapes are modeled as spheres (with Mie theory) and as irregular, cubelike particles with a semi-empirical model (19). The refractive index used is 1.31 for pure ice or $1.31 - 0.001i$ for ice with a small dissipative component added. In spite of this large variety of assumptions, the implied volume of dust in a burst generally falls in the range 4 to 200 m³, corresponding to a sphere 1 to 4 m in radius.

Studies of hypervelocity impacts show a linear relation between the mass of an impactor and the mass of the ejected dust, with typical yield factors of $10^{4\pm 1}$ (20). Assuming a comparable density for the impactor and the ejecta, the impactors must therefore have radii of 2 to 40 cm. The only plausible source of impactors in this size range is meteoroids falling in from outside the Saturn system.

The flux of centimeter-sized meteoroids at Saturn is not well known. Current observational constraints come from interpolations between Pioneer 10/11 meteoroid detector data applying to the 10- μm range (21), from known populations of Centaur (Saturn-crossing) asteroids in the 10- to 100-km range, and also from extrapolations outward of better data on meteoroid impacts acquired in the vicinity of Earth. Recent modeling pegs this flux at $10^{-18\pm 1.5} \text{ m}^{-2} \text{ s}^{-1}$ (22), depending on the meteoroid radius chosen, as a one-sided flux that neglects the focusing caused by Saturn’s gravity. This focusing factor is also poorly known. Tiny dust near Saturn is predominantly on cometary orbits that are focused by factors of 2 to 3, whereas larger bodies follow more circular, Centaur-type orbits that are focused by factors of ~ 50 . Adopting a focusing factor of 3 to 30, the flux at the F ring is $10^{-17\pm 2} \text{ m}^{-2} \text{ s}^{-1}$.

To predict the rate of impacts, we also need the ring’s cross section in bodies large enough to produce a visible burst. For this purpose, the Voyager radio science (RSS) occultation data are most useful because they observed the ring with the longest wavelength λ ; in general, an occultation experiment is sensitive to particles with $r \geq \lambda/2\pi$. The RSS experiment reveals the ring’s radially integrated optical depth W as 140 and 75 m for $\lambda = 3.6$ and 13 cm, respectively

(7). Extrapolating to $\lambda \approx 6$ m (appropriate for detecting only meter-sized ring particles) implies $W \sim 20$ m, for a total two-sided ring area of $2 \times 10^{10} \text{ m}^2$. Given the flux and the ring’s cross section, one ring impact of the necessary size should take place every 60 days, with an uncertainty of a factor of ~ 100 in either direction. The observed rate of once every 20 days falls well within this predicted range.

The above calculations reveal that meteoroid impacts are a plausible explanation for the burst events observed, although the numbers are uncertain. The cratering record on planets and moons attests to the frequency of impacts, but the witnessing of such events is rare on Earth and almost unknown elsewhere in the solar system.

It has long been recognized that meteoroid impacts can play a role in Saturn’s ring system. The influx of meteoritic material drives the compositional (22, 23) and orbital (24) evolution of the rings. Impact ionization and vaporization are probably also responsible for the rings’ thin “atmosphere” (25, 26). However, the most marked and visible manifestations of meteoroid impacts are probably the so-called “spokes” in Saturn’s B ring (2, 3, 20, 27). In most models, spokes are triggered by a meteoroid impact, after which the ejected dust becomes electrically charged and then propagates by interactions with the local plasma and magnetosphere (28–30); however, the details of these interactions remain unsettled, and at least one alternative model does not require any impactor (31). Reports of spoke patterns recurring at Saturn’s rotation rate (27) also suggest that impacts might not be required. Because the physics of burst events is so much simpler, the F ring provides less ambiguous evidence for ongoing impact processes in Saturn’s rings.

The cross section of the B ring is $\sim 2 \times 10^6$ times larger than that cited above for the F ring. If a 10-cm meteoroid strikes a body in the F ring every 20 days, then a similar meteoroid should strike the B ring every second. For comparison, spokes have been observed to form at the rate of one every ~ 600 s (32). This difference is understandable if the impactor needed to produce a spoke is larger, perhaps ~ 1 m based on estimates of the slope of the meteoroid size distribution (22) and on the amount of plasma needed to form a spoke (20, 28). However, many spokes straddle synchronous orbit R_{syn} , where ring particles corotate with Saturn’s magnetic field, and some models (28) suggest that only impacts occurring close to R_{syn} can form such two-sided spokes. In this case, the observed rate of two-sided spoke formation would imply that smaller (and therefore more frequent) impactors are required.

Over the long term, one might expect impacts to steadily erode away the F ring. However, this scenario depends on the ultimate destiny of the dust ejected. As noted above, dynamical models suggest that material spreads radially by ~ 100 km, a distance that encompasses the entire F ring but no other bodies except (rarely) Prometheus. Thus, the majority of the ejecta eventually recollides with the ring, and little material is permanently lost. Dust ejected from an F ring particle will continue to pass through the ring plane twice on each orbit, with one of those passages close to the ring. If an ejected grain sticks to the first ring particle it strikes and the ring has a mean optical depth of 0.05 to 0.1 (7), then the typical survival lifetime of ejected dust is 10 to 20 orbits or 7 to 14 days. This result compares favorably with the ~ 2 -week burst lifetimes observed (Fig. 2).

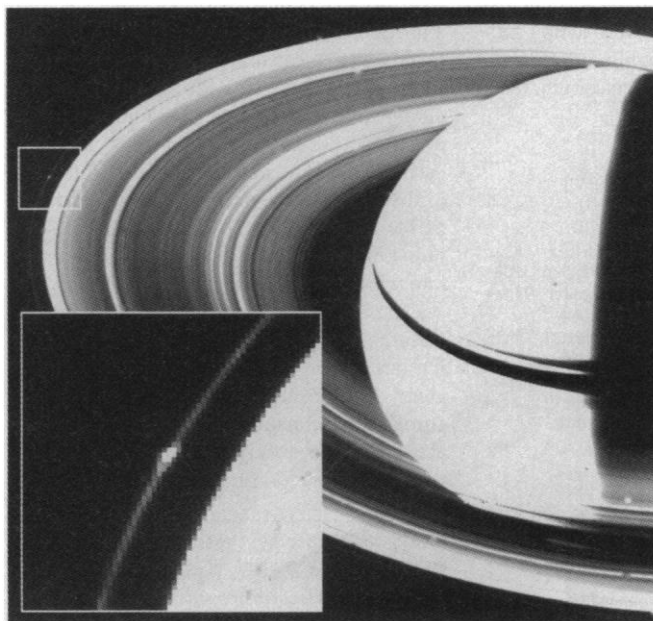


Fig. 3. Voyager image 44095.44 shows the most prominent time-variable clump, 2A (box). This same feature is shown enlarged and with enhanced contrast in the inset. At finest resolution, it shows a radial width of ~ 100 km in excess of the rest of the F ring; other, longer lived clumps do not show this enhanced width, ruling out the camera’s point spread function as being responsible.

With an observed detection every 20 days, the F ring appears to be the solar system's most sensitive detector of meteoroids in the 10-cm size range. Given the number of rings known, this may seem surprising. Several ring properties work together to make this so. First, the F ring is both narrow and optically thin, so an injection of a few cubic meters of dust is an observable event. A similar amount of material injected into a broader but faint ring such as the C ring or Cassini division would pass unnoticed. Second, with typical optical depths of ~ 0.1 , the ring is optically thick enough to represent a substantial target for impactors; most analogous rings, such as Saturn's E and G rings, are fainter by many orders of magnitude. Third, because the ring is narrow, an ejected dust grain is less likely to recollide with a large particle during each passage through the ring plane; as a result, the lifetime of a burst event is enhanced. In reality, narrow ringlets embedded in the Maxwell and Titan gaps of the C ring may serve as comparable detectors but were not as well observed by Voyager.

The flux of meteoroids has importance for the formation of the ring systems and the lifetimes of satellites. Results for the F ring raise the possibility that, by better calibrating our "detector," we could place new and important constraints on the flux of meteoroids in this intermediate size range. Further observations by the Hubble Space Telescope or the Cassini Orbiter should make this possible. Furthermore, a closer look at the F ring should reveal the more frequent, smaller bursts that were presumably overlooked in this analysis, possibly yielding the slope of meteoroid influx throughout the 1- to 100-cm range. It may also be possible to detect an asymmetry in the longitudes where bursts originate, as would be predicted by some models of meteoroid bombardment (20); this asymmetry, in turn, could shed light on whether the projectiles are approaching Saturn on cometary or Centaur-like orbits, with implications for their dynamical origin.

References and Notes

1. T. Gehrels *et al.*, *Science* **207**, 434 (1980).
2. B. A. Smith *et al.*, *ibid.* **212**, 163 (1981).
3. B. A. Smith *et al.*, *ibid.* **215**, 504 (1982).
4. S. F. Dermott, *Nature* **290**, 454 (1981).
5. M. R. Showalter and J. A. Burns, *Icarus* **52**, 526 (1982).
6. R. A. Kolvoord, J. A. Burns, M. R. Showalter, *Nature* **345**, 695 (1990).
7. M. R. Showalter, J. B. Pollack, M. E. Ockert, L. Doyle, J. B. Dalton, *Icarus* **100**, 394 (1992).
8. J. A. Burns, M. R. Showalter, G. Morfill, in *Planetary Rings*, R. Greenberg and A. Brahic, Eds. (Univ. of Arizona Press, Tucson, AZ, 1984), pp. 200–272.
9. A. S. Bosh and A. S. Rivkin, *Science* **272**, 518 (1996).
10. P. D. Nicholson *et al.*, *ibid.*, p. 509.
11. C. Roddier *et al.*, *IAU Circular* **6515** (1996).
12. M. R. Showalter, *Bull. Am. Astron. Soc.* **26**, 1150 (1994).
13. S. P. Synnott, R. J. Terrile, R. A. Jacobson, B. A. Smith, *Icarus* **53**, 156 (1983).
14. Intervals were 1 to 12 days, depending on image availability.

15. M. R. Showalter, *Bull. Am. Astron. Soc.* **29**, 999 (1997).
16. J. N. Cuzzi and J. A. Burns, *Icarus* **74**, 284 (1988).
17. F. Poulet and B. Sicardy, *Bull. Am. Astron. Soc.* **29**, 1001 (1997).
18. Grains larger than 100 μm make a negligible contribution in all except the very flattest size distributions.
19. J. B. Pollack and J. N. Cuzzi, *J. Atmos. Sci.* **37**, 868 (1980).
20. J. N. Cuzzi and R. H. Durisen, *Icarus* **84**, 467 (1990).
21. D. H. Humes, *J. Geophys. Res.* **85**, 5841 (1980).
22. J. N. Cuzzi and P. R. Estrada, *Icarus* **132**, 1 (1998).
23. L. R. Doyle, L. Dones, J. N. Cuzzi, *ibid.* **80**, 104 (1989).
24. R. H. Durisen *et al.*, *ibid.* **124**, 220 (1996).
25. G. E. Morfill, H. Fechtig, E. Grün, C. K. Goertz, *ibid.* **55**, 439 (1983).
26. D. T. Hall, P. D. Feldman, J. B. Holberg, M. A. McGrath, *Science* **272**, 516 (1996).

27. E. Grün, G. E. Morfill, R. J. Terrile, T. V. Johnson, G. Schwehm, *Icarus* **54**, 227 (1983).
28. C. K. Goertz and G. E. Morfill, *ibid.* **53**, 219 (1983).
29. G. E. Morfill, E. Grün, C. K. Goertz, T. V. Johnson, *ibid.*, p. 230.
30. M. Tagger, R. N. Henriksen, R. Pellat, *ibid.* **91**, 297 (1991).
31. J. R. Hill and D. A. Mendis, *J. Geophys. Res.* **87**, 7413 (1982).
32. E. Grün, G. W. Gameau, R. J. Terrile, T. V. Johnson, G. E. Morfill, *Adv. Space Res.* **4** (no. 4), 143 (1984).
33. I thank J. Cuzzi, L. Dones, and J. Lissauer for helpful discussions and comments and E. Duxbury and A. Wasserman of the Planetary Data System Imaging Node for extensive help with obtaining the data. Supported by NASA's Planetary Geology and Geophysics program through grant 344-30-51-05.

20 July 1998; accepted 7 October 1998

Neptune's Partial Rings: Action of Galatea on Self-Gravitating Arc Particles

Heikki Salo* and Jyrki Hänninen

Numerical simulations of Neptune's arcs show that self-gravity between macroscopic arc particles can prevent interparticle impacts and thereby stabilize their resonant confinement by Galatea, a satellite of Neptune. Stable subkilometer arc particles provide a source for replenishing the observed dust and explain the clumpy substructure seen in arcs. A few confining kilometer-sized particles between the major arc components can account for the observed arc widths spanning several resonance sites. The modeled distribution of dust is consistent with observations and helps to explain how embedded satellites may affect the structure and evolution of planetary ring systems.

Voyager 2 detected partial rings (arcs) around Neptune in August 1989 (1), confirming earlier Earth-based stellar occultation observations (2). The observed dusty material is concentrated in four 4°- to 10°-wide arcs (3), with a total azimuthal span of 40°. The arcs, with optical depths of about $\tau_a \sim 0.1$ are embedded in a diffuse Adams ring ($\tau_d \sim 0.003$) at a mean distance $a = 62,932$ km from Neptune. Arcs contain unresolved clumps of bright objects, containing dust (radius $r < 100 \mu\text{m}$) and larger ($r > 100 \mu\text{m}$) particles (4). The dust contributes 50 to 95% of the total τ of the arcs (5). The radial width of the arcs is $W_a \approx 15$ km, and they show radial distortion with amplitudes of about 30 km, while for the diffuse ring, $W_d \approx 50$ km.

The geometry and kinematic behavior of the arcs was explained by the resonant forcing due to the satellite Galatea, which orbits about 980 km inside the arcs (6). Its 42:43 corotation-inclination resonance (CIR) generates $2m_c = 86$ evenly spaced corotation sites around the ring (7). The guiding centers

(mean positions) of particles librate around these sites, which correspond to local maxima in the gravitational potential (δ). The nearby (~ 1.5 km inward of CIR) 42:43 outer Lindblad resonance (OLR) forces particles to have closed orbits in the reference frame of Galatea and is responsible for the observed radial distortions of the arcs.

Strictly speaking, the resonance model is only valid for macroscopic particles. Besides Galatea's perturbations dust grains are affected by radiation forces. The grains with $r < 100 \mu\text{m}$ are removed from CIR sites and possibly also from the diffuse ring in less than 100 years, because of solar radiation pressure (9). However, larger grains in CIR sites are shielded from the secular effects of Poynting-Robertson (PR) drag, whereas outside the sites, PR drag will drive them toward OLR which will increase their eccentricities (9). For example, icy grains will reach $e \sim W_d/a$, corresponding to the width of Adams ring, on time scales $T_{\text{Adams}} \sim 3 \times 10^3 (r/100 \mu\text{m})$ years. These short time scales suggest that the dust observed in CIR sites, and in the diffuse ring, is continuously replenished by impacts between macroscopic arc particles, which are unaffected by radiation forces. This scenario does not stabilize the arcs, however,

Division of Astronomy, Department of Physical Sciences, University of Oulu, FIN-90570 Oulu, Finland.

*To whom correspondence should be addressed. E-mail: hsalosun3@oulu.fi